Progress In Electromagnetics Research, Vol. 125, 327–341, 2012

SIMULATION ANALYSIS OF THE EFFECT OF MEASURED PARAMETERS ON THE EMISSIVITY ESTIMATION OF CALIBRATION LOAD IN BISTATIC REFLECTION MEASUREMENT

D. Liu*, K. Liu, M. Jin, Z. Li, and J. Miao

The School of Electronic and Information Engineering, Beihang University, Beijing 100191, China

Abstract—This paper presents the estimation of emissivity of calibration load using discretized scattering simulation data in bistatic reflection measurement, and analyzes the effect of several measured parameters on emissivity of calibration load. In the analysis of the impact of measured parameters on emissivity, a new calibration target is designed to improve the accuracy of emissivity measurement. In this bistatic measurement, the scattering from calibration load is simulated by FDTD (Finite-Difference Time-Domain) method. Based on Kirchhoff's law, the emissivity of calibration load is estimated by the discretized scattering data composed of different scanning angle interval and sampling azimuth planes. By the studies of simulation results, the estimation accuracy of emissivity of calibration load can be improved by selected appropriate measured parameters in bistatic reflection measurement.

1. INTRODUCTION

The absolute accuracy of microwave radiometers is very important for quantitative remote sensing. In order to achieve the higher accuracy of microwave radiometry, the calibration load-blackbody is generally used to provide brightness temperature reference to the radiometry. Usually the electromagnetic and physical properties of calibration load are widely studied [1–3], and the design and manufacture of blackbody are of concern [4–6]. However few studies investigate the measurement of emissivity of calibration load which

Received 6 January 2012, Accepted 27 February 2012, Scheduled 2 March 2012

* Corresponding author: Dawei Liu (dwliu@buaa.edu.cn).

is essential for industrial application. The emissivity of calibration load can be measured either directly or indirectly. The direct method requires measurement of the radiation emitted from a sample of known temperature. Sometimes, the temperature of sample is difficult to be obtained. The indirect method can be chosen alternatively, which measures the reflectivity of calibration load, and its emissivity is deduced from the reflectivity by use of Kirchhoff's law. In addition, there are two general types of indirect measurement. One is called monostatic measurement system [7, 8], in which only the backscattering power of the calibration load is measured to estimate the emissivity of calibration load. Using this method, the accuracy of emissivity will be influenced. Different from monostatic measurement, bistatic measurement [9], the other method, measures not only the backscattering, but also the scattering from the other direction [10–12]. Bistatic scattering in the space is measured to improve the estimated accuracy of emissivity of the calibration load. Although the bistatic measurement can improve the measurement accuracy of emissivity to some degree, it also needs a complex process in measurement, which demands optimization of scanning angle interval and sampling azimuth plane of measurement [13, 14].

In this paper, we will concentrate on the estimation of emissivity of calibration load in bistatic measurement. By the simulation, we study the effect of several measured parameters on the emissivity. Section 2 introduced the fundamental theory used in the estimation of emissivity in measurement. Section 3 provided the simulation results, which include measurement conditions, measured parameters and the analysis of results.

2. THEORY AND METHOD

In this section, the differential scattering coefficient and Kirchhoff's law are introduced, which are widely used in the estimation of emissivity [15–17]. The estimation of emissivity used in this section is presented as follows.

2.1. Estimation Method of Emissivity of Calibration Load

Assuming that the surface of target is rough enough, the radiation incident from upper half space can be scattered to the direction of (θ_s, ϕ_s). Fig. 1 showed the relationship of the incident and scattering wave. Differential scattering coefficient can be defined as below [16]

$$\gamma(\theta_0, \phi_0; \theta_s, \phi_s) = \frac{4\pi R^2 S_s}{S_0 A \cos\theta_0} \tag{1}$$

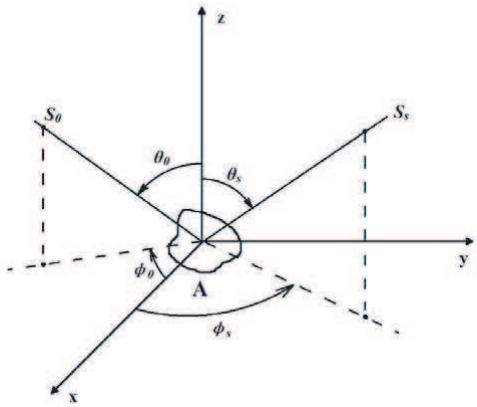

Figure 1. Schematic of the incident and scattering wave.

where (θ_0, ϕ_0) denotes the direction of incident wave, and (θ_s, ϕ_s) denotes the direction of scattering wave.

The reflectivity $A(\theta_0, \phi_0)$ of surface A can be expressed as

$$A(\theta_0, \phi_0) = \int \frac{R^2 S_s}{S_0 A \cos\theta_0} d\Omega_s \tag{2}$$

where $d\Omega_s$ donates the solid angle of scattering wave.

The horizontal polarized wave is discussed firstly, and the vertical polarization is similar to the horizontal polarized.

Both the horizontal and vertical polarization contribute to the scattering, so the equation as follows can be gotten,

$$\frac{R^2 S_s}{S_0 A \cos\theta_0} = \gamma(0, s) = [\gamma_{hv}(0, s) + \gamma_{hh}(0, s)] \frac{1}{4\pi} \tag{3}$$

Considering the total polarization in the totally upper half, the reflectivity can be improved to

$$A_h(\theta_0, \phi_0) = \frac{1}{4\pi} \int_{2\pi} [\gamma_{hh}(0, s) + \gamma_{hv}(0, s)] d\Omega_s \tag{4}$$

According to the thermodynamic equilibrium, absorptivity can be obtained

$$\alpha_h(\theta_0, \phi_0) = 1 - A_h(\theta_0, \phi_0) = 1 - \frac{1}{4\pi} \int_{2\pi} [\gamma_{hh}(0, s) + \gamma_{hv}(0, s)] d\Omega_s \tag{5}$$

Furthermore based on Kirchhoff's law, the emissivity in a certain polarization is equal to the absorptivity with the same polarization,

which can be expressed as

$$e(\theta_0, \phi_0) = \alpha(\theta_0, \phi_0) \tag{6}$$

From the above deduction, the relationship between emissivity and differential scattering coefficient can be derived from the Equations (5) and (6).

$$e_h(\theta_0, \phi_0) = \alpha_h(\theta_0, \phi_0) = 1 - \frac{1}{4\pi} \int_{2\pi} [\gamma_{hh}(0, s) + \gamma_{hv}(0, s)] d\Omega_s \tag{7}$$

Similarly, the emissivity in vertical polarization is the following,

$$e_v(\theta_0, \phi_0) = 1 - \frac{1}{4\pi} \int_{2\pi} [\gamma_{vv}(0, s) + \gamma_{vh}(0, s)] d\Omega_s \tag{8}$$

2.2. Fundamental Method of Estimation of Emissivity in Measurement

If the distribution of scattering field from calibration load is symmetrical, the emissivity of horizontal polarization can be estimated from scattering field in one azimuth angle. The Equation (7) can be denoted as follows,

$$\begin{aligned} e_h(\theta_0, \phi_0) &= 1 - \frac{1}{4\pi} \int_0^{2\pi} d\phi \int_0^{\frac{\pi}{2}} [\gamma_{hh}(0, s) + \gamma_{hv}(0, s)] \sin\theta d\theta \\ &= 1 - \frac{1}{2} \int_0^{\frac{\pi}{2}} [\gamma_{hh}(0, s) + \gamma_{hv}(0, s)] \sin\theta d\theta \end{aligned} \tag{9}$$

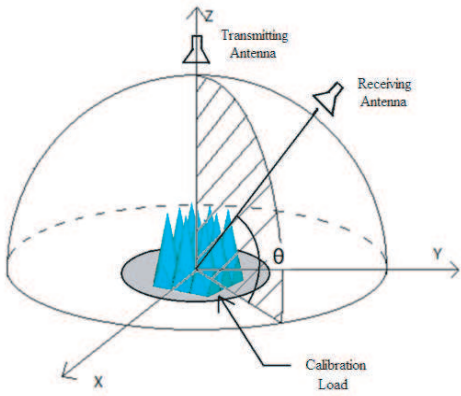

Figure 2. Schematic diagram of the estimation of emissivity in one sampling plane.

The Equation (9) is the fundamental formula applied in emissivity estimation. However in practical measurement, the scattering power from the whole space is difficult. Usually what we can measure are the discrete data. Sometimes only one sampling azimuth angle (in this paper, we call this sampling azimuth angle sampling plane) will be gotten in the measurement (shown as Fig. 2).

Under this situation, the discrete data are measured, and the scanning angle interval is determined. Thus, the equation should be described by Equation (10).

$$e_h(\theta_0,\phi_0) = 1-\frac{1}{2}\sum_{i=1}^{n}[\gamma_{hh}(\theta_0,\phi_0;\theta_i,\phi_{s1}) + \gamma_{hv}(\theta_0,\phi_0;\theta_i,\phi_{s1})]\sin\theta_i\Delta\theta \tag{10}$$

If, in one measurement, several sampling planes located on the angle $\phi_{s1},\phi_{s2},\ldots,\phi_{sn}$ can be measured, we can estimate the emissivity of calibration load using Equation (11).

$$e_h(\theta_0,\phi_0) = 1-\frac{1}{2n}\sum_{j=1}^{n_2}\sum_{i=1}^{n_1}[\gamma_{hh}(\theta_0,\phi_0;\theta_i,\phi_{sj}) + \gamma_{hv}(\theta_0,\phi_0;\theta_i,\phi_{sj})]\sin\theta_i\Delta\theta \tag{11}$$

where, ϕ_{si} denotes the angel in ith sampling plane (shown as Fig. 3), and n_2 denotes the total number of sampling planes.

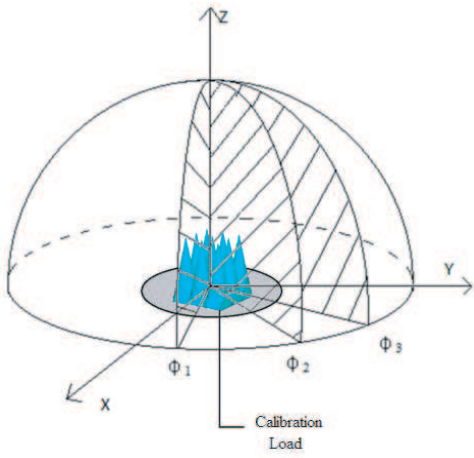

Figure 3. Schematic diagram of the estimation of emissivity in several sampling planes.

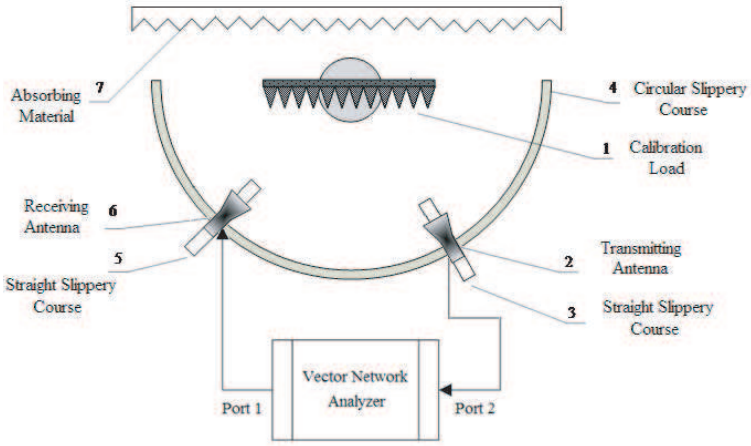

Figure 4. The measurement system of bistatic near field scanning in a circular orbit.

In practical measurement, we need to use the calibrated target to calibrate the calibration load-blackbody. The Equation (11) will be expressed as Equation (12),

$$e_h(\theta_0,\phi_0) = 1 - \frac{\frac{1}{2n}\sum_{j=1}^{n_2}\sum_{i=1}^{n_1}\left[\gamma_{hh}(\theta_0,\phi_0;\theta_i,\phi_{sj})+\gamma_{hv}(\theta_0,\phi_0;\theta_i,\phi_{sj})\right]\sin\theta_i\Delta\theta}{\frac{1}{2n}\sum_{j=1}^{n_2}\sum_{i=1}^{n_1}\left[\gamma'_{hh}(\theta_0,\phi_0;\theta_i,\phi_{sj})+\gamma'_{hv}(\theta_0,\phi_0;\theta_i,\phi_{sj})\right]\sin\theta_i\Delta\theta} \tag{12}$$

where γ'_{vv} and γ'_{vh}denote the corresponding reflectivity of calibration target.

3. SIMULATION OF THE EMISSIVITY MEASUREMENT OF CALIBRATION LOAD

In this paper we adopt the measurement system of bistatic near field scanning in a circular orbit as shown in Fig. 4 to simulate the emissivity of calibration load in horizontal polarization. The transmitted Gaussian beam illuminates on the surface of calibration load perpendicularly, and the reflected wave is received in the circular orbit.

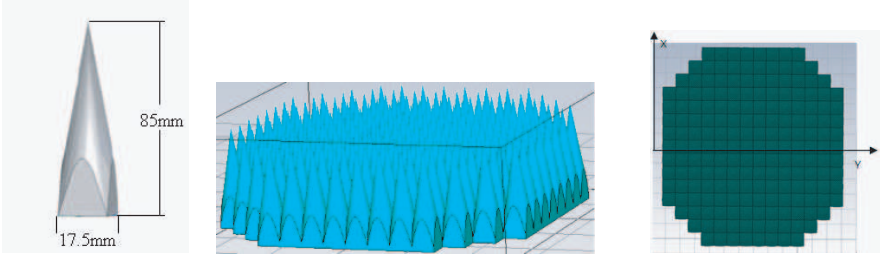

(a) (b) (c)

Figure 5. The structure of calibration load. (a) Structure of a circular cone unit. (b) Arrangement of the units (side view). (c) Arrangement of the units (vertical view).

The shape of calibration load measured in this simulation is designed the finite periodic array which is composed of many circular cone units with absorbing material as shown in Fig. 5. The Fig. 5(a) is the model of unit cone in the calibration load, and it can be obtained by removing the circular edge. The bottom of unit cone is square to ensure that they can be connected easily. The size of periodic array unit is 17.5 mm × 17.5 mm × 85 mm (17.5 mm is side length of the square, and 85 mm is the height of unit cone). The totally number of array units is 186, and the arrangement of the cone units is shown in Fig. 5(b) and Fig. 5(c). The composition of absorbing material is ECCOSORB®CR112. The surface of the calibration load and the calibration target is very smooth. In practical measurement, we need to use the calibration target to calibrate the blackbody which we study. In this simulation of measurement, the calibration load is made completely of absorbing materials, and calibration target is made of perfect metal. The calibration target is used to calibrate the blackbody-calibration load. The emitting wave is Gaussian beam [17], which illuminates in the center of the array perpendicularly. The noise of measurement system is not considered in the simulation process.

In this study, the scattering characteristic of calibration load is calibrated using FDTD method [18, 19]. FDTD method was presented first by K. S. Yee [20] in 1966, which was widely applied in electromagnetic scattering and propagation of the target with complex shape [21–24].

The simulation provides differential scattering coefficient, $\gamma_{hh}(0, s)$ and $\gamma_{hv}(0, s)$ of the circular cone units. And then, the Equations (10) (11) and (12) are used to calculate emissivity of the calibration load.

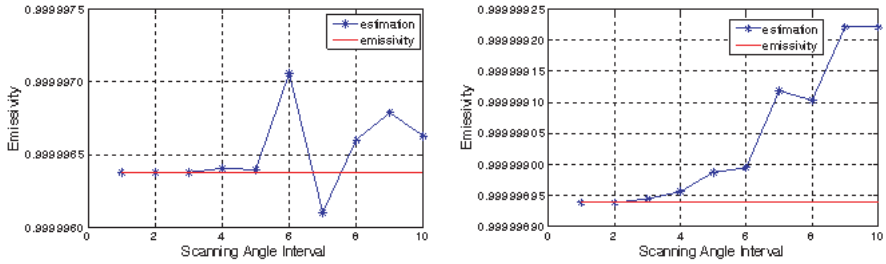

Figure 6. (a) The estimation of emissivity when $\phi = 0°$ (10.65 GHz). (b) The estimation of emissivity when $\phi = 45°$ (10.65 GHz.)

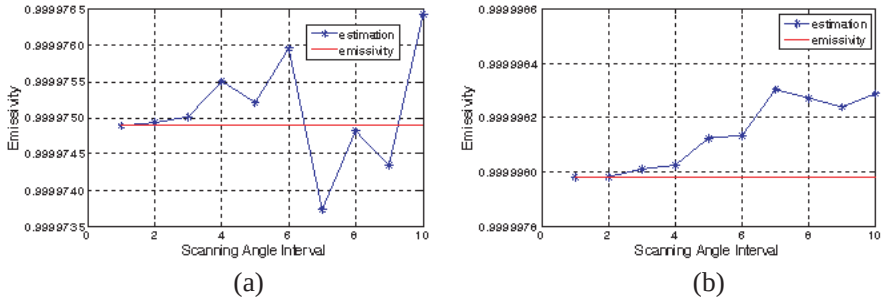

Figure 7. (a) The estimation of emissivity when $\phi = 0°$ (18.7 GHz). (b) The estimation of emissivity when $\phi = 45°$ (18.7 GHz).

3.1. The Effect of the Scanning Angle Interval on the Estimation of Emissivity

In the practical measurement, we hope to obtain the emissivity close to the true value through dense scanning angles. However, a large number of scanning angle require much measurement time, as a result the efficiency is limited in a great extent. In addition, dense scanning angles are limited by laboratory equipments. Here, the effect of scanning angle interval on estimation of emissivity of blackbody will be studied, and a reasonable angle interval considering both accuracy and efficiency is discussed.

In this simulation, several frequencies of incident wave are selected, which are 10.65 GHz, 18.7 GHz, 23.8 GHz and 36.5 GHz, respectively. The scanning angle is shown in Fig. 1, where θ is the angle measured in a sampling plane. When scanning angle interval is set to 1°, θ

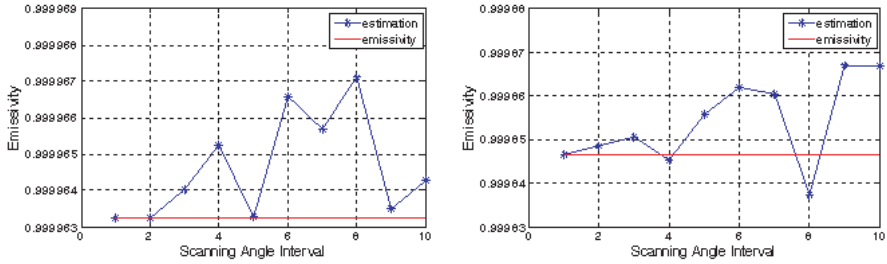

Figure 8. (a) The estimation of emissivity when $\phi = 0°$ (23.8 GHz). (b) The estimation of emissivity when $\phi = 45°$ (23.8 GHz).

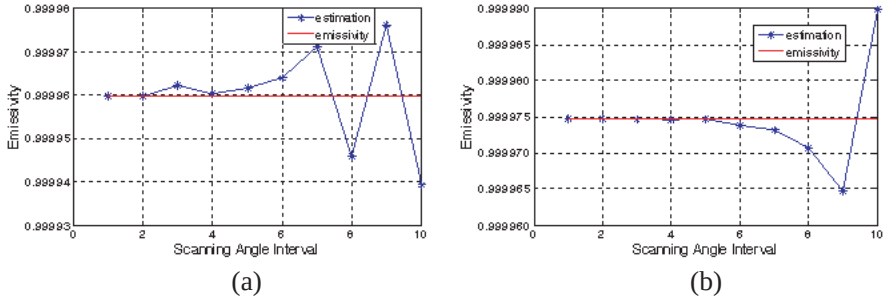

Figure 9. (a) The estimation of emissivity when $\phi = 0°$ (36.5 GHz). (b) The estimation of emissivity when $\phi = 45°$ (36.5 GHz).

is changed one by one from 0°, 1° ... to 90°. If it is set to 2°, θ will change by 2° from 0°, 2° ... to 90°. The rest can be deduced from this. The sampling plane is set in two directions $\phi = 0°$ and $\phi = 45°$.The Equation (10) is applied to estimate emissivity. The results of estimation are shown in Figs. 6–9.

In Figs. 6–9, the dot lines show the estimation of emissivity with different scanning angle interval in a certain sampling plane ($\phi = 0°$ or $\phi = 45°$), and the straight lines show the true value of emissivity estimation on the same plane. With the comparison of the both value, the influence of scanning angle interval will be clearly presented. From these figures, we can see that when the angle interval is small (about 1° or 2°), the estimation values is close to the ideal value obviously. But when the interval increases more than 4°, the values estimated appear serious fluctuation from the true ones.

A smaller angle interval may bring more accurate results of estimation. However, the dense scanning anglers are limited by measurement instruments and time in practical operation. From above simulation, we know that when the angle interval is not too large, the estimation is closed to the true value. From this simulation, we know that the angle interval 1° or 2° is more desirable in the measurement.

3.2. The Effect of the Sampling Plane on the Estimation of Emissivity

In this simulation, the effect of sampling planes on measurement accuracy is analyzed. The Equation (11) is applied to estimate emissivity. From this equation, we know that the emissivity of calibration load can be simulated by different sampling plane (the angle φ). According to the number of sampling planes, three cases

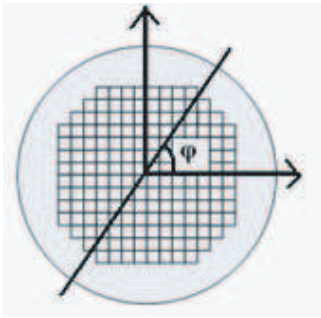

Figure 10. The azimuth angle of sampling plane.

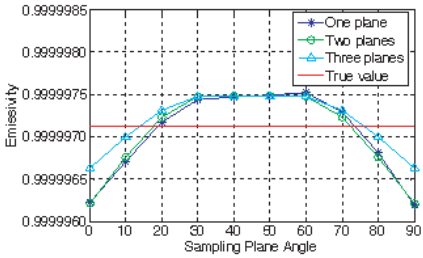

Figure 11. Effect of sampling plane (10.65 GHz).

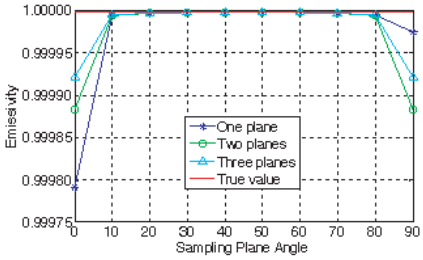

Figure 12. Effect of sampling plane (18.7 GHz).

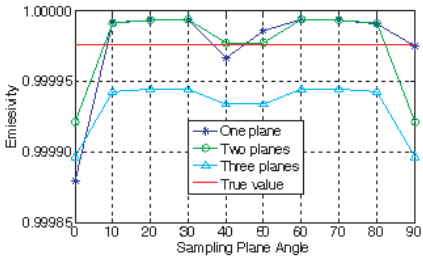

Figure 13. Effect of sampling plane (23.8 GHz).

are discussed, from one sampling plane, two sampling planes to three sampling planes. The angle ϕ denotes different position of the plane (as shown in Fig. 10). In the case of one sampling plane, we select the angle from $\phi = 0°$, $\phi = 10°, \ldots$, to $\phi = 90°$. The angle interval of sampling plane is 10°. For two sampling planes, we select the two angles which are complementary, from $\phi = 0°$ and $\phi = 90°$ as the first group, $\phi = 10°$ and $\phi = 80°$ as the second group, ... , to $\phi = 90°$ and $\phi = 0°$ as the last group. For the last case, three sampling planes are composed of two complementary angles and the angle $\phi = 45°$, from $\phi = 0°$, $\phi = 90°$, and $\phi = 45°$, $\phi = 10°$, $\phi = 80°$, and $\phi = 45°$, ..., to $\phi = 90°$, $\phi = 0°$, and $\phi = 45°$ in each group.

In this simulation the frequencies of incident wave are still 10.65 GHz, 18.7 GHz, 23.8 GHz and 36.5 GHz. Fig. 11–14 show the emissivity estimation of different sampling plane in these frequencies.

In these cases from Fig. 11 to Fig. 14, it can be seen that although two or three sampling planes don't improve the accuracy of the estimation of emissivity too much in Fig. 13 and 14, it can provide more stabled estimation. To some extent, this means that increasing in number of sampling planes can decrease the uncertainty of measurement. So in the measurement, we can select different sampling planes to estimate the emissivity of calibration load according to different acquirement in practical operation.

3.3. The Effect of the Calibrate Body on the Estimation of Emissivity

This simulation analyzes the effect of calibration target on measurement accuracy. Usually, in practical measurement, the calibration target is used to improve the estimation of emissivity of calibration load-blackbody. In traditional calibration method, metal

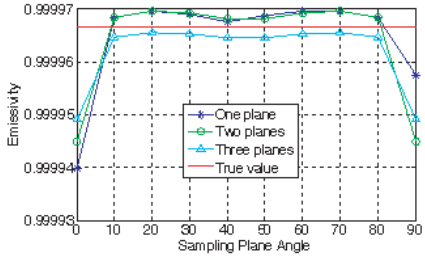

Figure 14. Effect of sampling plane (36.5 GHz).

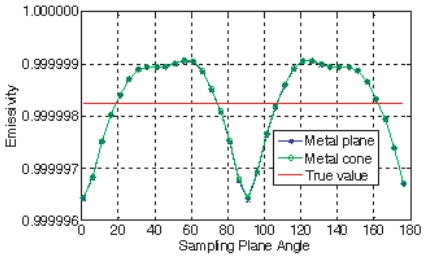

Figure 15. Effect of calibration target (10.65 GHz).

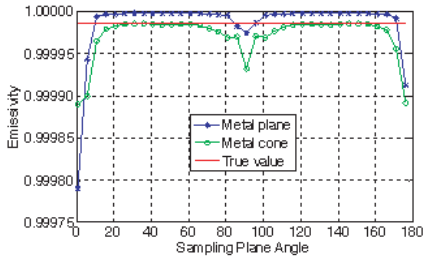

Figure 16. Effect of calibration target (18.7 GHz).

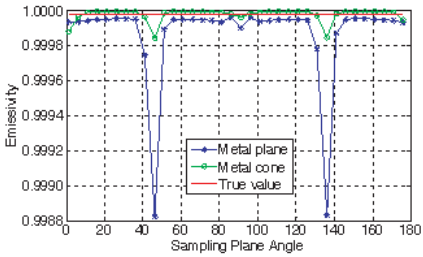

Figure 17. Effect of calibration target (23.8 GHz).

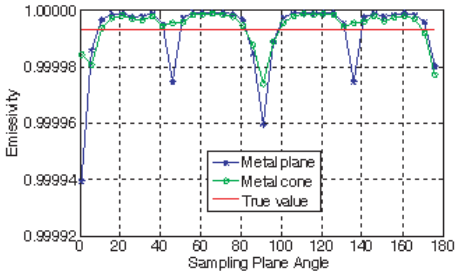

Figure 18. Effect of calibration target (36.5 GHz).

plate is often applied as calibrated target. This simulation presents another new calibration target-finite metal periodic cones array whose shape is the same as the blackbody which we study. The Equation (12) is used to estimate the emissivity of calibration load. To test the feasibility of the new calibrated target, three kinds of emissivity data are shown in the Figs. 15–18, the emissivity of true value, the one calibrated by metal plate, and the one calibrated by finite metal periodic cones array, respectively.

From the simulation result, it can be seen that the estimation accuracy is improved. For the frequency 23.8 GHz and 36.5 GHz, the performance of new calibration target is more apparent. But, for the lower frequency 10.65 GHz, two calibration targets have almost the same performance. Since the scattering characteristic of new calibration target is similar to the traditional in the lower frequency, they have the similar performance. So from this simulation, it can be known that when frequency is higher, the performance of new calibration target will be better.

4. CONCLUSION

This paper analyzes the influence of incomplete measurement data on the estimation of emissivity in two-dimension bistatic measurement system. Through the discussion of angular interval, sampling plane and calibration target, the relationship between estimation and true are presented in numerical simulation. In the practical measurement, it is suggested that the interval of scanning angle may be less than 2° as well and more sampling planes should be used to estimate the emissivity of calibration load. Finally, a new calibration target with the same corn unit as the calibration load-blackbody is applied in the estimation of emissivity, which can improve the accuracy of emissivity estimation in situation of high frequency.

REFERENCES

1. Wang, J., J. Miao, Y. Yang, and Y. Chen, "Scattering property and emissivity of a periodic pyramid array covered with absorbing material," *IEEE Transactions on Antennas and Propagation*, Vol. 56, No. 8, 2656–2663, 2008.
2. De Roo, R. D., *Theory and Measurement of Bistatic Scattering of X-band Microwaves from Rough Dielectric Surfaces,* The University of Michigan, America, 1996.
3. Zahn, D. J., *Investigation of Bistatic Scattering Using Numerical Techniques and Novel Near-field Measurements,* The University of Michigan, America, 2001.
4. Wollack, E. J., D. J. Fixsen, A. Kogut, M. Limon, P. Mirel, and J. Singal, "Radiometric-waveguide calibrators," *IEEE Transactions on Instrumentation and Measurement*, Vol. 56, No. 5, 2073–2078, 2007.
5. Lambrigtsen, B. H., "Calibration of the AIRS microwave instruments," *IEEE Transactions on Geoscience and Remote Sensing*, Vol. 41, No. 2, 369–378, 2003.
6. Jones, W. L., J. D. Park, S. Soisuvarn, H. Liang, P. W. Gaiser, and K. M. S. Germain, "Deep-space calibration of the WindSat radiometer," *IEEE Transactions on Geoscience and Remote Sensing*, Vol. 44, No. 3, 476–495, 2006.
7. Lonnqvist, A., A. Tamminen, J. Mallat, and A. V. Raisanen, "Monostatic reflectivity measurement of radar absorbing materials at 310 GHz", *IEEE Transactions on Microwave Theory and Techniques*, Vol. 54, No. 9, 3486–3491, 2006.

8. Tamminen, A., A. Lonnqvist, J. Mallat, and A. V. Raisanen, "Monostatic reflectivity and transmittance of radar absorbing materials at 650 GHz," *IEEE Transactions on Microwave Theory and Techniques*, Vol. 56, No. 3, 632–637, 2008.
9. Bellez, S., H. Roussel, C. Dahon, and J. M. Geffrein, "A rigorous forest scattering model validation through comparison with indoor bistatic scattering measurements," *Progress In Electromagnectics Research B*, Vol. 33, 1–19, 2011.
10. Currie, N. C., N. T. Alexander, and M. T. Tuley, "Unique calibration issues for bistatic radar reflectivity measurements," *Proceedings of the 1996 IEEE Radar Conference*, 1996.
11. Matkin, B. L., J. H. Mullins, T. J. Ferster, and P. J. Vanderford, "Bistatic reflectivity measurements at X, Ku, Ka and W-band frequencies," *Proceedings of the 2001 IEEE Radar Conference*, 2001.
12. Li, F., J. Miao, D. Zhao, and Z. Li, "A simulation study on the blackbody emissivity measurement using bistatic radar," *ISAPE '06, 7th International Symposium on Antennas, Propagation & EM Theory*, 2006.
13. Smith, F. C., B. Chambers, and J. C. Bennett, "Tolerance in the measurement of RAM reflectivity," *ICAP 91, Seventh International Conference on Antennas and Propagation*, 1991.
14. Zhang, H., D. Plettemeier, J. Miao, B. C. Wu, and M. Bai, "Parametric optimization of microwave radiometer calibration load," *Asia-Pacific Symposium on Electromagnetic Compatibility and 19th International Zurich Symposium on Electromagnetic Compatibility, APEMC 2008,* 2008.
15. Wang, J., Y. Yang, J. Miao, and Y. Chen, "Emissivity calculation for a finite circular array of pyramidal absorbers based on Kirchhoff's law of thermal radiation," *IEEE Transactions on Antennas and Propagation*, Vol. 58, No. 4, 1173–1180, 2010.
16. Zhang, Z. and S. Lin, *Microwave Measurement Technique and Application,* Publishing House of Electronics Industry, Beijing, 1995.
17. Li, J., Y. Chen, S. Xu, Y. Wang, M. Zhou, Q. Zhao, Y. Xin, and F. Chen, "Vectorial structure of a phase-flipped gauss beam in the far-field", *Progress In Electromagnetics Research B*, Vol. 26, 237–256, 2010.
18. Teixeira, F. L., "Time-domain finite-difference and finite-element methods for Maxwell equations in complex media," *IEEE Transactions on Antennas and Propagation*, Vol. 56, No. 8, 2150–2166, 2008.

19. Chen, C. Y., Q. Wu, X. J. Bi, Y. M. Wu, and L. W. Li, "Characteristic analysis for FDTD based on frequency response," *Journal of Electromagnetic Waves and Application*, Vol. 24, No. 2, 283–292, 2010.
20. Yee, K. S., "Numerical solution of initial boundary value problems involving Maxwell equations in isotropic media," *IEEE Transactions on Antennas and Propagation*, Vol. 14, No. 3, 302–307, 1966.
21. Shibayama, J., A. Yamahira, T. Mugita, J. Yamauchi, and H. Nakano, "A finite-difference time-domain beam-propagation method for TE-and TM-wave analyses," *Journal of Lightwave Technology*, Vol. 21, No. 7, 1709–1715, 2003.
22. Vaccari, A., A. Cala' Lesina, L. Cristoforetti, and R. Pontalti, "Parallel implementation of a 3D subgridding FDTD algorithm for large simulations," *Progress In Electromagetics Research*, Vol. 120, 263–292, 2011.
23. Tay, W. C. and E. L. Tan, "Implementations of PMC and PEC boundary conditions for efficient fundamental ADI- and LOD-FDTD," *Journal of Electromagnetic Waves and Application*, Vol. 24, No. 4, 565–573, 2010.
24. Li, J., L.-X. Guo, and H. Zeng, "FDTD method investigation on the polarimetric scattering from 2-D rough surface," *Progress In Electromagnetics Research*, Vol. 101, 173–188, 2010.